

Key Points:

- A floating optical buoy (FOBY) designed to measure water-leaving radiance directly based on the skylight-blocked approach was developed
- FOBY-derived remote sensing reflectance showed better performance than that from a PSR in terms of data quality and stability
- The uncertainties of FOBY-derived R_{rs} may result from self-shading, sensor tilt, and the immersed depth of the cone (IDC)

Correspondence to:

S. Li and J. Zhao,
 lisen9368@whu.edu.cn;
 zhaojun28@mail.sysu.edu.cn

Citation:

Tian, L., Li, S., Li, Y., Sun, Z., Song, Q., & Zhao, J. (2020). A floating optical buoy (FOBY) for direct measurement of water-leaving radiance based on the skylight-blocked approach (SBA): An experiment in Honghu Lake, China. *Journal of Geophysical Research: Oceans*, 125, e2020JC016322. <https://doi.org/10.1029/2020JC016322>

Received 15 APR 2020

Accepted 8 OCT 2020

Accepted article online 12 OCT 2020

A Floating Optical Buoy (FOBY) for Direct Measurement of Water-Leaving Radiance Based on the Skylight-Blocked Approach (SBA): An Experiment in Honghu Lake, China

Liqiao Tian¹ , Sen Li¹, Yong Li¹, Zhaohua Sun², Qingjun Song^{3,4}, and Jun Zhao^{5,6} 

¹State Key Laboratory of Information Engineering in Surveying, Mapping, and Remote Sensing, Wuhan University, Wuhan, China, ²State Key Laboratory of Tropical Oceanography, South China Sea Institute of Oceanology, Chinese Academy of Sciences, Guangzhou, China, ³Ministry of Natural Resource of the People's Republic of China, National Satellite Ocean Application Service, Beijing, China, ⁴Key Laboratory of Space Ocean Remote Sensing and Application, Ministry of Natural Resource of the People's Republic of China, Beijing, China, ⁵School of Marine Sciences, Sun Yat-sen University, Guangzhou, China, ⁶Southern Laboratory of Ocean Science and Engineering, Zhuhai, China

Abstract Water-leaving radiance (L_w), or remote sensing reflectance (R_{rs}), is a fundamental parameter of water color remote sensing. However, obtaining accurate and precise measurements of L_w is quite challenging. This study is intended to illustrate the design and implementation of a novel floating optical buoy (FOBY) to measure L_w directly in the field based on the skylight-blocked approach (SBA). To assess the performance of FOBY, an experiment was conducted in Honghu Lake, China, a typical shallow turbid lake. FOBY-derived R_{rs} can characterize the spectral features of different water types including water with kelp as substrate, relatively high chlorophyll-a contents, and high amounts of suspended sediment (SS). FOBY-derived R_{rs} is superior to that from a portable spectroradiometer (PSR 3500+, Spectral Evolution Inc.) based on the conventional above-surface approach (ASA) in terms of data quality and stability. FOBY measurements had a quality assurance score (QAS) of 0.98 and a mean coefficient of variation (CV) of 3.6–7.0%, while the mean CV for PSR measurements is more than 2 times larger than that of FOBY in the visible domain. The measurement uncertainties may result from self-shading, sensor tilt, and the immersed depth of the cone (IDC), which deserve further investigations. In the future, long-term continuous floating observations of different aquatic environments can be conducted using the instrument with well-refined data quality control.

Plain Language Summary Aimed at accurate and precise in situ measurements of water-leaving radiance (L_w) or remote sensing reflectance (R_{rs}), a floating optical buoy (FOBY) was developed to measure L_w directly based on the skylight-blocked approach in this paper. An experiment was conducted in Honghu Lake, China. Our results demonstrated less variability of R_{rs} from FOBY than from the traditional above-surface approach. On the other hand, it should be noted that uncertainties of R_{rs} from FOBY still exist and deserve further investigations. In the future, FOBY can serve for long-term continuous observations of different aquatic environments with well-refined data quality control.

1. Introduction

Satellite remote sensing can provide views of aquatic environments with its capabilities of synoptic and repetitive coverage over large spatial and temporal scales, even in inaccessible regions by human beings (Gregg et al., 2005; Groom et al., 2019). With the availability of different types of satellite data products, long-term changes or trends of biogeochemical parameters can be well unraveled (Dunstan et al., 2018; Marrari et al., 2017). On these grounds, the effects of climate change and anthropogenic activities on aquatic environments can be revealed (Dutkiewicz et al., 2019). However, the good accuracy of satellite-derived data products is a prerequisite for the credibility of the derived information.

Water-leaving radiance (L_w) or remote sensing reflectance (R_{rs}) is a key parameter for water color remote sensing. It provides fundamental inputs for many retrieval algorithms. To obtain accurate and reliable satellite products, keeping radiometric uncertainty below 5% at 443 nm for clear waters is scientifically required and high calibration accuracy is also desired in inland turbid waters (IOCCG, 2012). However,

the achievement of this long-standing goal is challenged by the accuracy of the system level calibration of satellite sensors (Zibordi et al., 2015). Satellite data calibration and reprocessing are needed because satellite instruments tend to degrade over time. For example, Moderate Resolution Imaging Spectroradiometer (MODIS) ocean color data have been reprocessed several times to incorporate advancements in instrument calibration (https://oceancolor.gsfc.nasa.gov/forum/oceancolor/topic_show.pl?tid=7817). Postlaunch calibration of satellite sensors mainly depends on in situ measurements. Although conventional ship-based measurements served the scientific community for decades, L_w from ship-of-opportunity is subject to uncertainties caused by reflection from hull and shadow. Long-term continuous measurements from optical buoys suffer from high operating and maintenance costs, such as the Marine Optical Buoy (MOBY), which has been the primary basis for the vicarious calibration of numerous ocean color sensors, like Sea-Viewing Wide Field-of-View Sensor (SeaWiFS), MODIS, and Visible Infrared Imaging Radiometer Suite (VIIRS), since 1996. The Aerosol Robotic Network-Ocean Color (AERONET-OC) network of the U.S. National Aeronautics and Space Administration (NASA) is also used for long-term field measurements to validate primary ocean color products (Zibordi et al., 2009) and can avoid biofouling. However, complex quality control processes are required for AERONET-OC data to eliminate surface reflection effects (Toole et al., 2000; Zibordi et al., 2004). The correction of surface-reflectance light is complicated, and uncertainties also exist in the procedure. Moreover, measurements from both research vessel and moored buoy have the limitation of sparse spatial or temporal coverage. Therefore, an alternative that can be deployed easily for long-term continuous floating observations of L_w is desired.

Traditional approaches derive L_w or R_{rs} via measuring various related components that are then used to calculate the key properties through postprocessing routines. They generally involve one of the following approaches: (1) All relevant properties are measured from an above-surface platform and then L_w is calculated by removing surface-reflected light (Hooker et al., 2004), (2) vertical profiles of upwelling radiance are measured and then the measurements are propagated upward across the water surface to obtain L_w (Smith et al., 1984), and (3) upwelling radiance from a sensor a few centimeters below the water surface is mathematically propagated across the surface to get L_w (Toole et al., 2000; Zibordi & Talone, 2020). Each of these approaches has discrete advantages and disadvantages (Garaba & Zielinski, 2013; Hooker et al., 2002; Ruddick et al., 2019). Ahn et al. (1999) introduced an approach to measure L_w directly, and Tanaka et al. (2006) tested a similar dome-covered apparatus to carry out direct L_w measurements. Lee et al. (2013) presented a hybrid scheme, the skylight-blocked approach (SBA), to avoid drawbacks of traditional approaches and achieved high precision results in Lake Michigan and Green Bay. The SBA scheme for L_w (and R_{rs}) has been tested and performed well in waters of various optical types (Castagna et al., 2020; Kutser et al., 2013, 2016; Wei et al., 2015, 2018). Compared with traditional schemes, the SBA scheme has at least two advantages: (1) It provides direct measurements of L_w without the procedures involved in deriving L_w from the above-surface method or underwater vertical profiles. For example, the correction of surface-reflected light or the extrapolation of radiance to derive L_w may introduce great uncertainties; (2) it is applicable to various types of aquatic environments, even very shallow waters. Nonetheless, the in-water approach is unsuitable in shallow waters and prominently affected by stratification, which can cause uncertainties in the extrapolation of vertical profiles of upwelling radiance ($L_u(z)$) to upwelling radiance just below the surface ($L_u(0^-)$). However, to date, there is no instrument specifically designed following SBA. Furthermore, the performance of SBA has not been tested in shallow turbid waters yet.

The present study describes a floating optical buoy (FOBY) instrument that was designed to measure L_w based on the SBA scheme. A field experiment was carried out during 23–28 March 2018 in Honghu Lake, China. Our goal was to test the performance of FOBY and assess data quality from the system.

2. Configuration of FOBY

Compared with the SBA scheme proposed by Lee et al. (2013), FOBY has been improved in the following aspects: (a) FOBY is designed by integrating two independent hyperspectral radiometers, which are placed in the middle, rather than on each side of the float. (b) A round shape of the floating body is used. This design is suitable for installation behind small or unmanned ships and can keep the whole system stable even during rough water states. (c) To meet the long-term operation goal in the future, a cleaning brush is attached

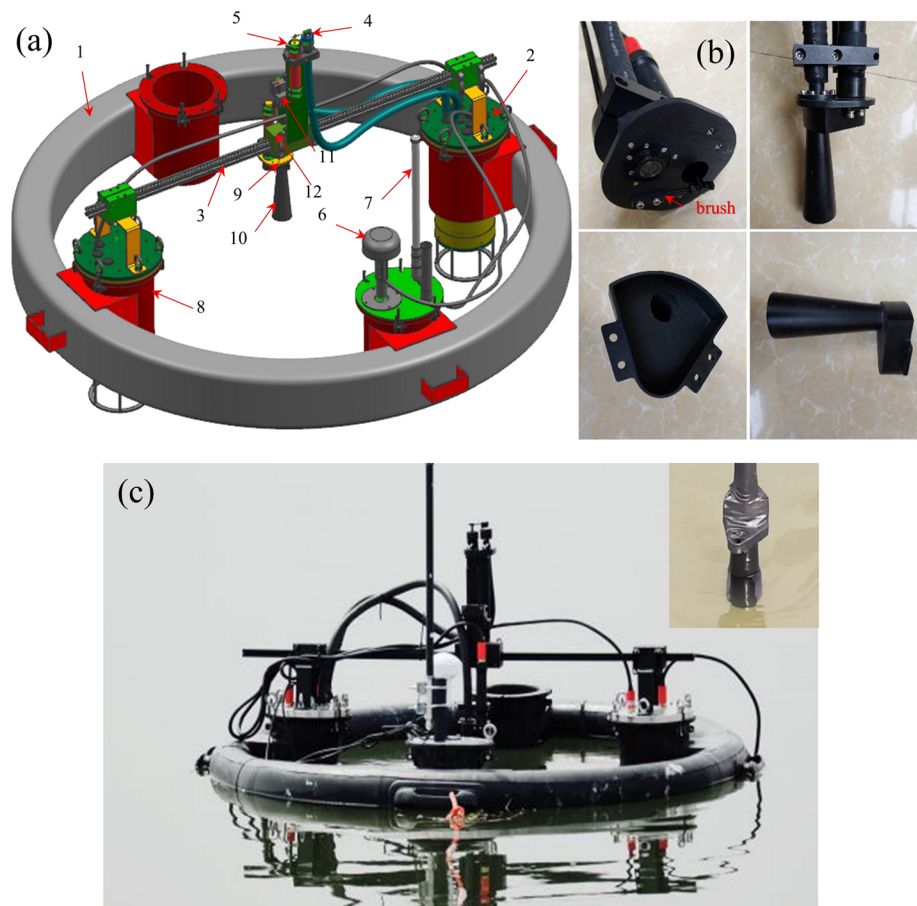


Figure 1. (a) Schematic of a floating optical buoy (FOBY): (1) floating collar, the main body of the FOBY; (2) data acquisition chamber; (3) cross girder; (4) irradiance sensor; (5) cleaning brush for the irradiance sensor; (6) GPS antenna; (7) wireless communication antenna; (8) battery chamber; (9) radiance sensor; (10) cone for the radiance sensor, the open end of which lies below the surface; (11) depth adjuster; and (12) fixing bracket. Components are illustrated in color for easy visualization; in real life, all components were painted black if required. (b) Detailed configuration of the radiance sensor with the brush annotated. (c) Picture of a FOBY deployed in the field with an inset picture showing the submerged cone of the radiance sensor.

beside the radiance sensor to test the function of avoiding the biofouling effects and removing water droplets on the surface of the sensor.

The structure of FOBY uses a modular design and mainly consists of four modules: the floating body, the data acquisition module, the positioning and transmission module, and the system control and power module. The schematic of FOBY is shown in Figure 1.

2.1. Floating Body

The floating body consists of a floating collar, four data acquisition chambers, and a cross girder. The floating collar has an inner diameter of 1.3 m and an outer diameter of 1.5 m with a width of 0.1 m. The large inner diameter and narrow hull can minimize the effects of self-shading. The whole body is painted black to reduce the effect of surface light. Besides, the floating body can be inflated for measurement and deflated for transportation. A picture of FOBY during our field survey is shown in Figure 1c.

2.2. Data Acquisition Module

In the present study, FOBY is designed by integrating two TriOS RAMSES radiometers (<https://www.trios.de/en/radiometers.html>), one for downwelling irradiance (E_d) and the other for upwelling radiance. Both sensors have been calibrated before and after field surveys according to protocols of the National Institute

of Metrology of China (Li, 2001). They can simultaneously measure E_d and L_w with a spectral increment of 3.3 nm between 368 and 881 nm. Since FOBY is deployed in water, the demand for watertightness is met. A black cone is connected to the radiance sensor that has a field of view (FOV) of 8° (Figure 1b). To ensure direct measurements of L_w , the open end of the 15 cm high, 5 cm diameter cone is designed to be inserted below the water surface at an adjustable depth. In this study, 2 cm was adopted as the immersed depth of the cone (IDC) to minimize the contamination caused by the shadow of the radiance sensor in turbid waters. The other end of the cone has a special shape as shown in Figure 1b. This configuration is designed to accommodate a brush to clean the surface of the radiance sensor. Tests in the laboratory have affirmed that the FOV of the radiance sensor is not affected by the special shape.

2.3. Positioning and Transmission Module

As shown in Figure 1, a GPS antenna and a wireless transmission antenna are attached to FOBY. They are both miniaturized to avoid being broken during field investigation. The GPS positioning component is used to record the latitude and longitude of each deployment. Its horizontal positioning accuracy is better than 2.5 m. The wireless transmission antenna works in the frequency range of 410–441 MHz. It can support data reception and command delivery between FOBY and the Ground Control System for about 3 km, which is far beyond the layout distance.

2.4. System Control and Power Module

The control system adopted a PCM-3363 processor. The processor is characterized by low power consumption which is no more than 13 W. The battery is installed in the battery chamber as shown in Figure 1a. The lithium battery is light in weight and has sufficient power which can meet the demands of continuous observation for more than 1 day.

3. Data and Method

3.1. Experiment Area

Honghu Lake, the seventh largest freshwater lake in China, covers an area of 348.2 km². The lake connects to the Yangtze River through a canal along its southeastern boundary. Honghu Lake is also a typical inland shallow turbid lake with an average depth of 1.4 m. The variations of chlorophyll-a (Chl-a) concentration, SS concentration, and colored dissolved organic matter (CDOM) in Honghu Lake are detailed in section 4.1. The lake is characterized by rich biological resources, especially submerged aquatic vegetation (SAV) consisting of *Potamogeton maackianus* A. Benn., *Myriophyllum spicatum* L., *Hydrilla verticillata* (L.f.) Royle, *Ceratophyllum oryzetorum* Kom., and *Potamogeton lucens* L. (Zhang, 1998). It serves as an important area for bird migration and breeding, as well as essential habitat for endangered species. Therefore, awareness of water properties in the region is of great importance. However, remote sensing of the aquatic environment and related field investigations has scarcely been reported in this area.

3.2. FOBY Data Collection and Processing

A field experiment was conducted on 23, 26, 27, and 28 March 2018 in Honghu Lake, China. The stations visited are shown in Figure 2. At each station, the FOBY was deployed more than 20 m away from the ship to minimize the reflection and shadowing of the ship hull. Each measurement was carried out after the ship totally stopped, and the water surface calmed down to avoid white-wash and ship wakes. For each deployment, 50 spectra of both L_w and E_d were recorded within 5 s synchronously. Given possible changes in the stability and calibration of FOBY's radiometers due to transportation or variations in adjacent conditions, radiance measurements using a standard diffuse reflector (Labsphere) were made on deck at each station. The flow chart of data collection and processing is shown in Figure 3. In total, 60 stations were investigated. Some of them were revisited on different days.

The methodology proposed by Lee et al. (2013) was adopted for FOBY data processing and is briefly described here. Data had to be removed when the radiance sensor was submerged below the water surface or when the cone was entirely above the surface. Contaminated data were identified through the following steps: (1) The median and standard deviation of L_w for wavelengths >750 nm were calculated, (2) the spectrally averaged value of L_w for the range of 750–800 nm was obtained, and (3) contaminated data were

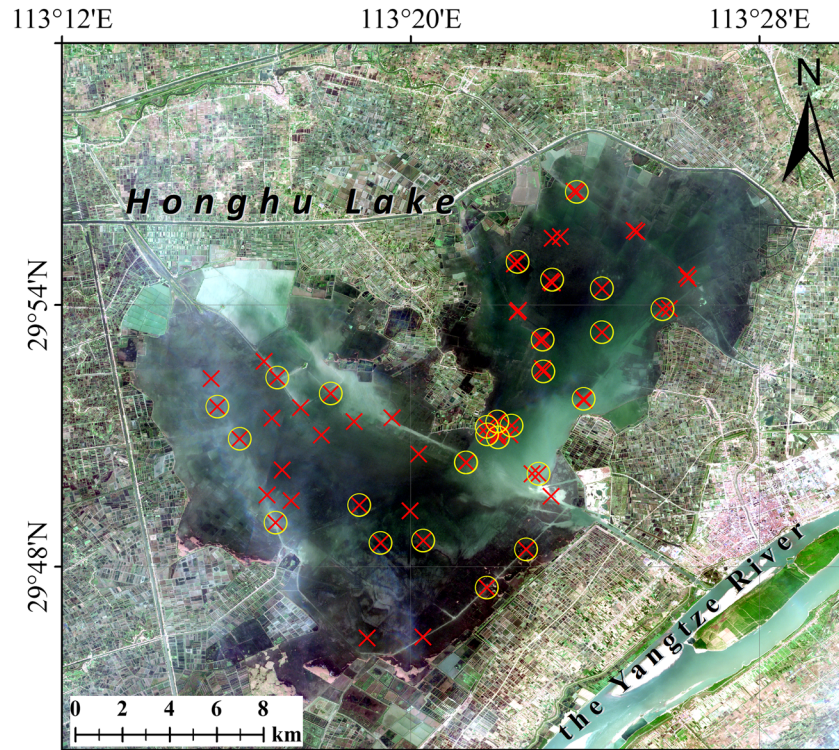


Figure 2. Map of the experiment area, Honghu Lake, China. Red “x” symbols show all stations investigated during a field survey between 23 and 28 March 2018. Open yellow circles show valid concurrent measurements by both the FOBY and a PSR 3500 + spectroradiometer.

recognized if the spectral mean is larger than the median plus three standard deviations. E_d data were also visually inspected to remove those sharp changes caused by shadow or cloud. R_{rs} was calculated from

$$R_{rs}(\lambda, t) = \frac{L_w(\lambda, t)}{E_d(\lambda, t)} \quad (1)$$

with λ for wavelength and t for the observation time.

Self-shading of the radiance sensor in FOBY is unavoidable. The self-shading correction algorithm proposed by Shang et al. (2017) was exploited in this study. The self-shading scheme was evaluated and supported using controlled experiment (Lin et al., 2020). The formulas are as follows:

$$\varepsilon = 1 - \exp\left(-K \frac{R}{\tan(\theta_w)}\right) \quad (2)$$

$$K(\lambda) = [3.15\sin(\theta_w) + 1.15]e^{-1.57b_b(\lambda)}a(\lambda) + [5.62\sin(\theta_w) - 0.23]e^{-0.5a(\lambda)}b_b(\lambda) \quad (3)$$

$$a(\lambda) = a_w(\lambda) + a_{ch}(\lambda) + a_s(\lambda) + a_g(\lambda) \quad (4)$$

$$b_b(\lambda) = b_{bw}(\lambda) + b_{bch}(\lambda) + b_{bs}(\lambda) \quad (5)$$

Here R is the radius of the cone, θ_w is the subsurface zenith angle of sunlight, a is the total absorption coefficient, and b_b is the total backscattering coefficient. Using Equations 2 and 3, self-shading corrections were applied to all R_{rs} data. R was set to 0.025 m according to the design of FOBY. θ_w was calculated using latitudes and longitudes of stations along with the corresponding times of in situ measurements. The subscripts w , ch , s , and g denote pure water, Chl-a, SS, and CDOM, respectively. a is the sum of absorption from the four optically active constituents, and b_b is the sum of backscattering from pure water, Chl-a, and SS. a_w and b_{bw} spectra of pure water were taken from Lee et al. (2015) and Mason et al. (2016). a_{ch} , b_{bch} , a_s , and b_{bs} was

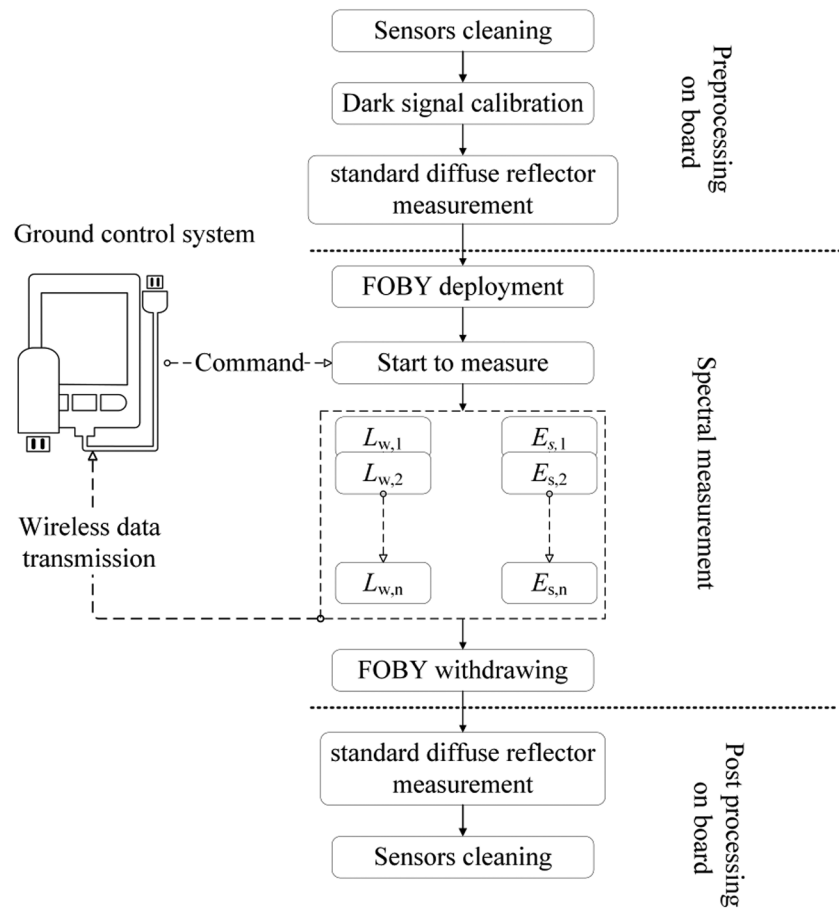


Figure 3. The flow chart of FOBY data collection.

expressed using the specific absorption or backscattering coefficients multiplied by the concentrations of Chl-a and SS, which were measured in the field (Lahet et al., 2000). Finally, the following equation was used to remove the contribution of self-shading to R_{rs} :

$$R_{rs}^{true} = \frac{R_{rs}^{shaded}}{1 - \varepsilon} \quad (6)$$

where R_{rs}^{shaded} denotes the R_{rs} derived by FOBY and R_{rs}^{true} denotes the “true” R_{rs} after self-shading correction.

3.3. PSR Data Collection and Processing

Along with FOBY, a portable spectroradiometer (PSR 3500+, Spectral Evolution, Inc., Lawrence, MA, USA) was used to collect R_{rs} following the above-surface approach (ASA). Hereafter, PSR will be used for short. The instrument covers a spectral range of 350–2,500 nm with a spectral resolution of 2.8 nm at 700 nm, 8 nm at 1500 nm and 6 nm at 2100 nm (<https://spectralevolution.com/products/hardware/field-portable-spectroradiometers-for-remote-sensing/psr/>). Total upwelling radiance above the water surface ($L_t(\lambda)$), downwelling sky radiance ($L_{sky}(\lambda)$), and “gray plaque” radiance ($L_p(\lambda)$) reflected from a standard diffuse reflector (Labsphere) were measured. At each station, 15 scans of $L_t(\lambda)$, $L_{sky}(\lambda)$, and $L_p(\lambda)$ were made for each loop, respectively, and 3 loops were carried out. The measurement geometry followed the NASA Ocean Optics Protocols (Mueller, 2003). A viewing direction of zenith angle $\approx 40^\circ$ from the nadir and of azimuth angle $\approx 135^\circ$ from the Sun was used for sky radiance measurements. With this observation geometry, the effects of Sun glint and nonuniform sky radiance could be minimized and instrument shading could be avoided (Mobley, 1999).

R_{rs} spectra were calculated from the following equations:

$$R_{rs}(\lambda) = \frac{L_w(\lambda)}{E_d(\lambda)} = \frac{[L_t(\lambda) - \rho(\lambda)L_{sky}(\lambda)]\rho_p}{\pi L_p(\lambda)} \quad (7)$$

where $L_w(\lambda)$ is spectral water-leaving radiance, $E_d(\lambda)$ is spectral downwelling irradiance, $\rho(\lambda)$ is the effective surface reflectance, and ρ_p is the reflectance of the gray plaque when viewed at a fixed angle. In the present study, $\rho(\lambda)$ varies with wavelength and is obtained utilizing a nonlinear spectral optimization method and a biooptical model. For detailed calculation formulas and steps, please refer to Cui et al. (2013) and Lee et al. (2010). Given the effects of cloud and boat movement, PSR measurements from 18 stations were retained for later analysis (Figure 2).

3.4. Concentrations of Optically Active Constituents

Surface water samples were collected with a polyethylene bucket. In the laboratory, water samples were filtered under low vacuum through Whatman GF/F filters with a pore size of 0.7 μm and stored in a refrigerator at -20°C until extraction. Pigments were extracted with 90% acetone. Chl-a was determined spectrophotometrically (Ritchie, 2006). Samples were also filtered through 0.45 μm preweighted polycarbonate filters. The filters were then dried at 40°C for 48 hours. SS was obtained by subtracting the weight of blank filters. To determine the absorption of CDOM, water samples were filtered through 0.22 μm polycarbonate filters. The filtered samples were scanned from 190 to 1,100 nm with a spectrophotometer (TU-1810PC, Persee General Instrument, Ltd. Beijing, China). Milli-Q water was used as a reference for baseline correction. For residual scattering correction, the average over a 5 nm interval around 685 nm was subtracted from the optical density spectrum (Babin et al., 2003). For details regarding CDOM determination, please refer to Zhao et al. (2018).

3.5. Other Data

During the entire observation period, meteorological parameters, including wind speed (0–5.3 m s^{-1}) and direction, were also recorded. To assess the R_{rs} data quality from FOBY, the quality assurance scheme developed by Wei et al. (2016) was implemented. A high-quality assurance score (QAS) indicates high data quality.

4. Results

4.1. Variations of Chl-a, SS, and CDOM in Honghu Lake

Honghu Lake is a typical shallow lake with various water types. Figure 4 shows the spatial distributions of Chl-a, SS, and CDOM absorption at 350 nm ($a_g(350)$) during the entire observation period. Chl-a concentration varied in a relatively large range from 0.74 to 40.38 $\mu\text{g L}^{-1}$, with high values in the northwestern part of the study area and low values in the southeastern part. High Chl-a was related to the inflow of freshwater that may carry nutrients to the lake, supporting the growth of phytoplankton. SS ranged from 0.35 to 95.2 mg L^{-1} . It was also high in the area where freshwater from upstream watersheds flowed into the lake. In addition, high SS was found along the shipping channel where boats passed by and stirred up the bottom sediment. $a_g(350)$ varied between 2.18 and 5.13 m^{-1} and showed a similar pattern to that of Chl-a except for that $a_g(350)$ was high along the shipping channel. The spectral slope of CDOM between 300 and 350 nm varied from 0.015 to 0.026 nm^{-1} . These results show good agreement with previous studies (Chen et al., 2009; Zhou et al., 2017).

4.2. R_{rs} Spectra From FOBY

Figure 5 shows the self-shading corrected R_{rs} spectra between 368 and 881 nm from FOBY for all stations. All spectra peak around 580 nm and vary from 0.0034 to 0.017 sr^{-1} , demonstrating a wide range of water types. A shoulder around 650 nm is also discernable, which is related to the strong absorption of chlorophyll-a and phycocyanin (PC) as well as the fluorescence of PC (Soja-Woźniak et al., 2017). The clear peaks of R_{rs} around 680–700 nm can be attributed to solar-induced chlorophyll-a fluorescence. The peak wavelength shifts toward longer wavelengths as Chl-a increases (Gitelson, 1993). This can be explained by the effects of the combined absorption by pigment and water with increased Chl-a (Schalles, 2006). The peaks around

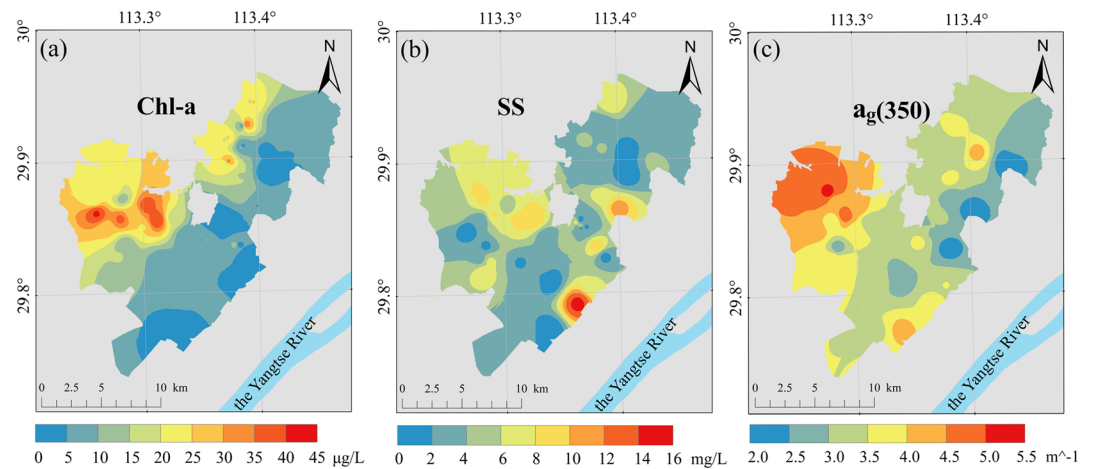


Figure 4. Maps of chlorophyll-a (Chl-a) concentration (a), suspended sediment (SS) concentration (b), and absorption of colored dissolved organic matter (CDOM) at 350 nm ($a_g(350)$) (c) during the observation period of 23–28 March 2018 in Honghu Lake, China.

710 nm are more influenced by the SAV substrate. These features are similar to those observed in Taihu Lake, bordered by Jiangsu and Zhejiang provinces, China (Ma et al., 2011).

R_{rs} spectra for representative water types observed in the study area are presented in Figure 6. Figures 6a and 6d show a field picture for waters with SAV and the corresponding R_{rs} spectrum, respectively. The spectral peak around 720 nm is even higher than R_{rs} in the green region. Similar characteristics were reported for waters with SAV (Visser et al., 2015; Yadav et al., 2017). Figures 6b and 6e display the field picture and the corresponding R_{rs} spectrum for green waters with Chl-a of $6.67 \mu\text{g L}^{-1}$, respectively. The spectrum is typical for turbid Case II waters with relatively high Chl-a. Figures 6c and 6f present the field picture and the corresponding R_{rs} spectrum for yellowish-brown waters with SS as high as 95.2 mg L^{-1} , respectively. R_{rs} values for this water type are generally larger than those of the other two water types.

4.3. Comparison of R_{rs} From FOBY and PSR

R_{rs} in the near-infrared and ultraviolet region is relatively low; thus, small fluctuations in ambient conditions may result in large uncertainties in R_{rs} . Therefore, later analysis focuses on the spectral domain of

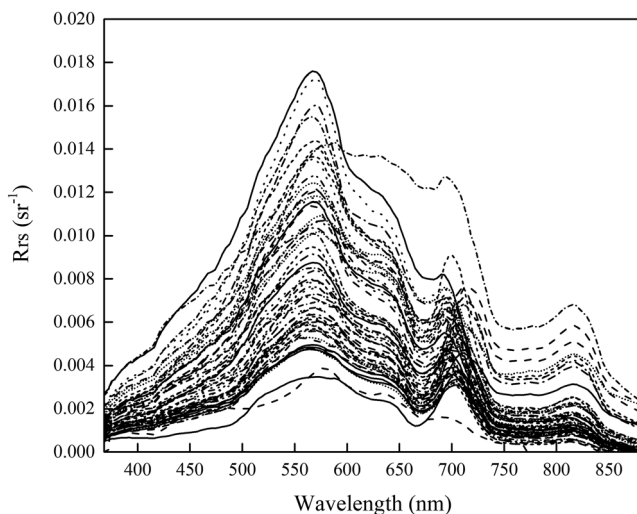


Figure 5. Remote sensing reflectance (R_{rs}) spectra collected by the FOBY for all stations investigated in Honghu Lake, China, shown in Figure 2.

400–750 nm. For all 18 stations with quality-controlled concurrent measurements from both FOBY and PSR, the statistical parameters, including coefficient of determination (R^2), slope, and intercept from linear regressions between R_{rs} from the two instruments, are shown in Figure 7. R^2 is >0.94 for 415–700 and 735–750 nm while <0.94 for other spectral ranges. The slope varied between 0.8 and 1.4. It was >1 for 400–585 and 735–750 nm, which indicated that R_{rs} from PSR was larger than that from FOBY. The slope was <1 for 585–750 nm, demonstrating smaller R_{rs} values from FOBY than from PSR. The intercept (Figure 7) ranged from -0.00032 and 0.0012 sr^{-1} . Given the complex optical properties of the investigated water and heterogeneous distributions of SAV and its anisotropic characteristics, these results demonstrate the validity of R_{rs} acquired from the two schemes.

To further evaluate R_{rs} from FOBY and PSR, coefficients of variation (CVs) for R_{rs} spectra of each station were calculated. CV is defined as the standard deviation divided by the average of R_{rs} calculated from multiple measurements. The CV spectra at a station with Chl-a concentration of $6.67 \mu\text{g L}^{-1}$ and SS concentration of 4.51 mg L^{-1} are shown in Figure 8. For FOBY-derived R_{rs} at this station, CV ranged from 1.58% to

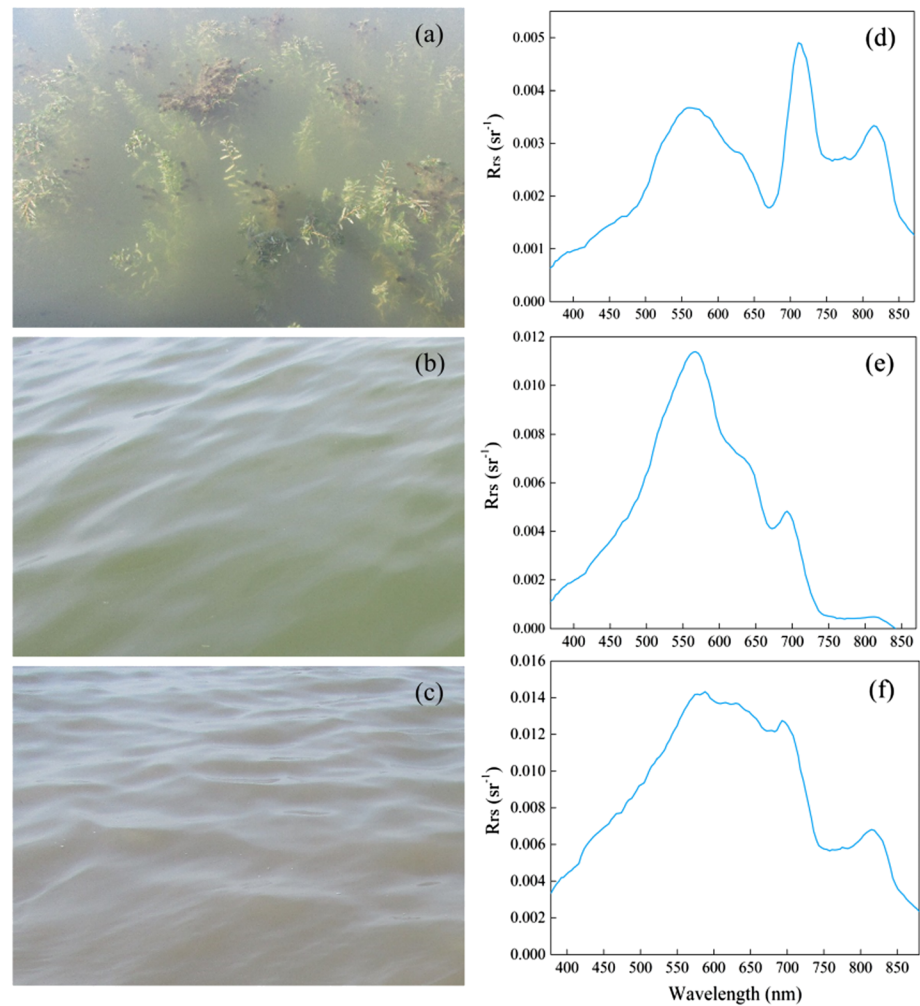


Figure 6. Field pictures (a–c) of different waters and their corresponding R_{rs} spectra (d–f) collected in Honghu Lake, China. Each pair of photos represents (a)/(d) water with a kelp substrate, (b)/(e) green water with a relatively high Chl-a, and (c)/(f) brown water with a high concentration of SS.

12.80% and was <5% for the spectral range of 400–730 nm. With respect to R_{rs} from PSR, CV varied from 4.01% to 11.20%. For the spectral range of 525–640 nm, CV from PSR was twice as large as that from FOBY. Comparisons of CVs between the two schemes at other stations demonstrated similar findings. Note that CV from FOBY was systematically smaller than that from PSR, demonstrating that the former scheme provided more precise results than the latter one. QAS (Wei et al., 2016) was calculated for the entire observation period. All QASs were higher than 0.98, which further shows the high quality of R_{rs} from FOBY.

To further highlight the higher precision of R_{rs} from FOBY than from PSR, the averaged CV spectra for stations with concurrent measurements from the two schemes were calculated and displayed in Figure 9. For R_{rs} from FOBY, the mean CV ranged from 3.6% to 7.0% for wavelengths shorter than 700 nm and <20% in the spectral range of 700–750 nm. For R_{rs} from PSR, the mean spectral CV was generally greater than that from FOBY. For wavelengths between 475 and 670 nm, the averaged CV from PSR ranged from 6.8% to 10.9%. For the shorter (400–475 nm) and longer (700–750 nm) wavelengths, the averaged CV reached 20.75% and 50.0%, respectively. The lower variability observed in FOBY data is consistent with the results observed by Lee et al. (2013). Note that the higher variability of R_{rs} from PSR can be partly attributed to the nonsimultaneous measurements of radiance for different targets. Simultaneous measurements can reduce the uncertainties of R_{rs} caused by environmental sources.

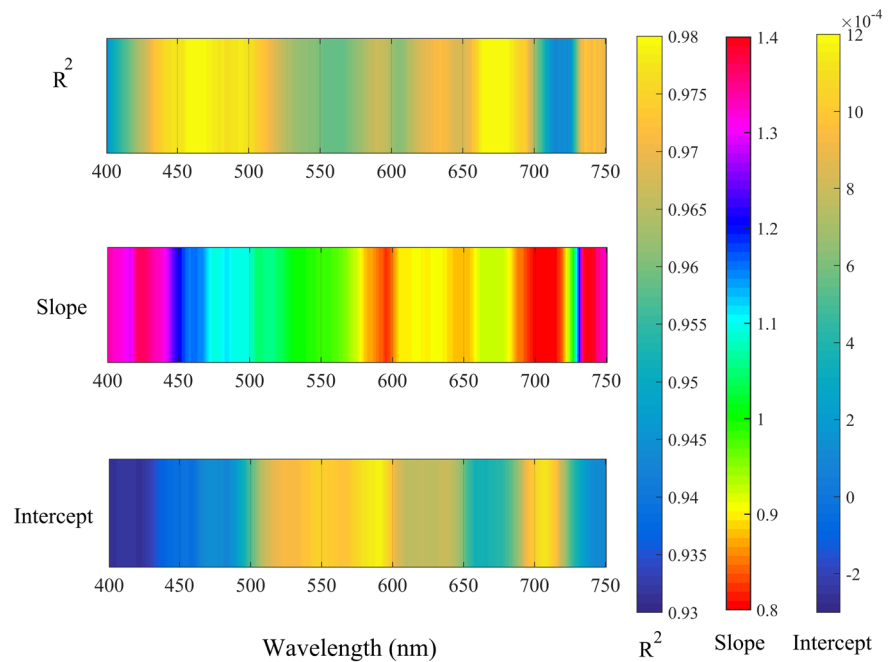


Figure 7. Comparison between the FOBY and PSR derived R_{rs} in the spectral range of 400–750 nm. R^2 , slope, and intercept derived from linear regressions are demonstrated here.

5. Discussion and Outlook

5.1. Advantages of SBA and FOBY

The goal of obtaining L_w with an uncertainty of less than 5% in the blue spectral domain in clear waters is widely accepted by the water color community. However, this has been proved difficult to achieve (Zibordi et al., 2002). It is also more challenging to obtain precise and accurate measurements of L_w in turbid waters. For decades, scientists have proposed different methodologies to improve the accuracy of L_w measurements. Hooker and Maritorena (2000) showed that the objective of producing L_w within an uncertainty of 5% in clear waters was achievable using in-water radiometry. However, their results were limited to measurements in oceanic waters, at local noon, and for the spectral range of 412–555 nm. Garaba and Zielinski (2013) compared R_{rs} from above and in-water measurements and showed that the uncertainty ranged from 5% to 110% in the 410–555 nm spectral range. Lee et al. (2013) compared L_w via SBA with that from in-water profiles. They found that SBA can provide high precision measurements of L_w and that the uncertainty of L_w within 5% can be attained in the spectral range of 400–650 nm. Their findings shed light on the high precision measurement of L_w , and thus, the long-standing objective of L_w uncertainty less than 5% is achievable when all other sources of random and systematic uncertainties can be addressed.

We developed a novel instrument, that is, FOBY, to directly measure L_w based on the SBA scheme, from which R_{rs} can be derived. Comparisons were also made for measurements from FOBY and PSR. R_{rs} from FOBY demonstrated higher precision than that from PSR. Together with other factors, such as rough sea surface, clouds, stratification of water column, and wave-induced light focusing, correction of surface-reflected light is critical for the acquisition of accurate R_{rs} data based on ASA. Mobley (1999) used radiative transfer numerical models to estimate ρ in a way that was dependent on sky conditions, wind speed, solar zenith angle, and viewing geometry. He suggested a wavelength-independent

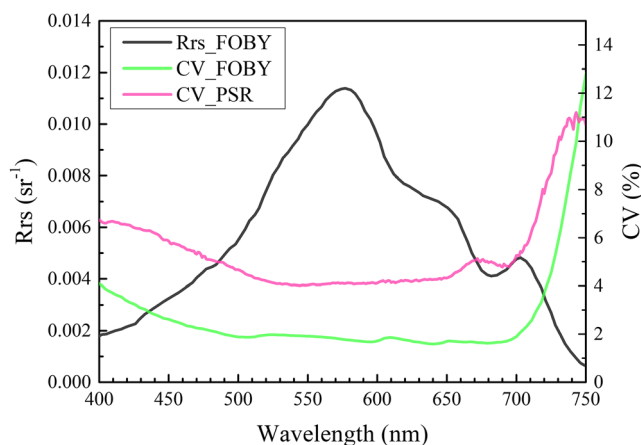


Figure 8. The coefficient of variation (CV) spectra of R_{rs} derived by the FOBY and the PSR at a station with Chl-a concentration of $6.67 \mu\text{g L}^{-1}$ and SS concentration of 4.51 mg L^{-1} . R_{rs} spectra from FOBY are also displayed here.

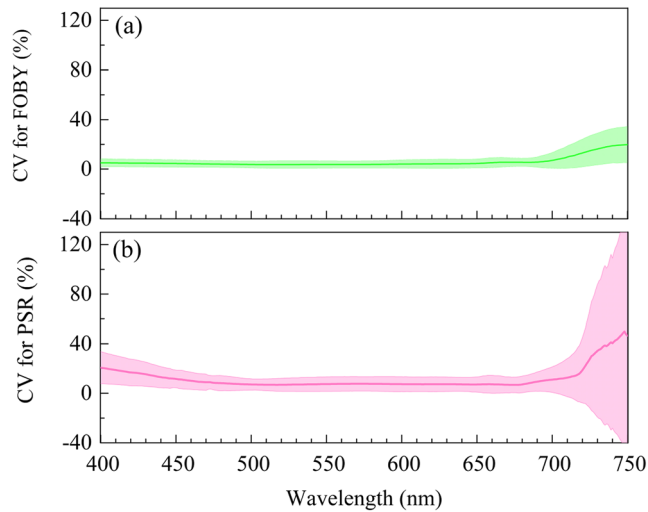


Figure 9. The mean CV spectra of R_{rs} for all concurrent measurements from the FOBY (a) and the PSR (b) in Honghu Lake, China. The shaded colors indicate the standard deviations.

value of $\rho \approx 0.028$ for wind speed less than 5 m s^{-1} . However, this is more appropriate for overcast sky conditions than for clear-sky conditions (Lee et al., 2010). Cui et al. (2013) proposed an approach to obtain ρ that was spectrally variable. Since ρ was related to wind speed, sky condition, solar zenith angle, and viewing geometry, it varied between different stations besides its spectral variability. Significant uncertainties occur when removing skylight reflection using the existing approaches. Conventional approaches for L_w also included measurements of upwelling radiance from in-water profiles or several centimeters below the water surface. However, these methods involved propagation through the air-water interface, which also introduced uncertainties. Because FOBY measured L_w directly, errors associated with the correction of surface-reflected light and propagation of upwelling radiance through the air-water interface can be avoided (Ruddick et al., 2019).

5.2. Uncertainties of FOBY Measurements

As demonstrated above, FOBY can provide L_w of high precision and low variability. Nevertheless, it should be noted that uncertainties also exist in FOBY data. Instrument self-shading is unavoidable, as can be seen in Figure 1b. Gordon and Ding (1992) and Leathers et al. (2001) proposed approaches to account for instrument shading effects on L_w . Their methods estimated instrument self-shading as a function of absorption coefficient, instrument size, and solar zenith angle. Zhao (2010) used Leathers et al.'s method to correct the instrument self-shading effect on L_w as measured in the turbid Pearl River estuary. Their results indicated that the instrument self-shading induced uncertainties of 2–9% in L_w . Shang et al. (2017) used Monte Carlo simulations to characterize the self-shading of a SBA system and found that the error caused by the instrument's self-shading varied in the range of ~1–20% for most water properties and solar positions. In this study, instrument self-shading was corrected to improve the accuracy of L_w measurements. By using a small FOV and a small aperture for the radiometer, the self-shading effect on R_{rs} from FOBY can be minimized (Lee et al., 2013).

Another potential source of uncertainty is from situations when the radiometer is submerged or when the cone rises above water surface. Data for these situations can be effectively removed based on data quality control as implemented in this study. R_{rs} contaminated under those situations is significantly higher than normal values because (1) the sensor measures upwelling radiance below water surface when it is submerged and (2) the measured signal is total upwelling radiance when the cone is above water surface. In this study, the open end of the black cone was inserted 2 cm below water surface in the turbid Honghu Lake. In Lake Michigan and Green Bay, Lee et al. (2013) used a depth of 5 cm below the surface instead. The black cone was integrated to block skylight and, meanwhile, not to interfere with the underwater light field. With lessons learned from our field surveys, the effects of IDC on R_{rs} may be small for clear waters while significant for turbid waters. However, how IDC affected R_{rs} from FOBY is still unknown. More experiments will be conducted to quantitatively investigate the effect of IDC on R_{rs} from FOBY under different wind and wave conditions. Protocols of measurement will be established to refine deployment and data processing to minimize the potential uncertainties caused by IDC (Ruddick et al., 2019).

In addition, wind-induced sensor tilt may result in uncertainties of FOBY-derived R_{rs} . Our field experiment was conducted in conditions with generally light winds. We found that CV of R_{rs} from FOBY under clear-sky conditions with wind speeds $< 2 \text{ m s}^{-1}$ was systematically smaller than that with wind speeds $> 2 \text{ m s}^{-1}$. It may be caused by the sensor tilt change on a relatively rough water surface, which led to apparent changes in the viewing angle of the E_d sensor. This is also likely associated with the fact that SS was stirred up in the shallow lake when the wind speed was large. However, due to the fact that most measurements were conducted in relatively calm waters, other factors, such as illumination, water type, and water substrate types, were not effectively controlled. To quantify the relationship between uncertainties of R_{rs} from FOBY and wind speed is beyond the scope of the present study. It deserves further investigations in the future.

5.3. Future Perspectives on FOBY

As demonstrated above, FOBY has great advantages for accurate measurements of L_w . It can be easily deployed over a wide range of environmental conditions. Using FOBY, the duration of individual measurements can be significantly shortened, which is very helpful for observing R_{rs} in shallow waters without perturbation of the water column. FOBY can provide long-term observations of R_{rs} at low cost for validation and calibration of satellite sensors and real-time continuous monitoring of water properties. Future versions of the system will be minimized, in part to minimize the self-shading of instrument. Meanwhile, the effect of depth, that is, the position where the open end of the black cone is immersed below water surface, on the FOBY performance will be investigated. A single-axis or dual-axis inclinometer will be installed to record the FOBY tilts which are indispensable for quality control (Lee et al., 2019). All sensors will be customized and installed according to individual needs. A cardanic gimbal will be mounted to stabilize the radiometers. A propeller vane will be outfitted in the system to adjust the position of FOBY for optimal measurements. A disposable FOBY could also be developed, which can drift with ocean circulations. Thus, optical properties of water masses and their small-scale features, such as submesoscale eddies, can be captured. Further, emerging water pollutants, such as microplastics (Garaba & Dierssen, 2018), can be characterized by their spectral signatures. By deploying a series of FOBYs, extreme events and their effects on aquatic environments can be investigated in detail, based on which efficient policies can be made to minimize potential economic losses and adverse effects on local ecosystems.

6. Conclusions

In this work, based on the SBA scheme, we developed a novel instrument, called FOBY, to measure L_w directly, which is a key property for hydrooptics and water color remote sensing. An experiment was carried out in Honghu Lake, China. Several water types, such as water with SAV, water with high chlorophyll-a contents, and water with high loads of SS, were investigated. FOBY demonstrated great precision, which can help with fulfilling the long-established objective of achieving a precision of L_w within 5%. Although FOBY has great prospects and advantages, the precision and accuracy of R_{rs} from FOBY are affected by self-shading of the radiometric sensor and swaying of FOBY's floating body under strong winds, causing irradiance change and immersion of the radiometric sensor in water or swinging of the cone in the air. The effects of IDC and wind speed on the uncertainties of R_{rs} from FOBY remain unclear and require additional studies. Extensive experiments in the field covering more water types will be conducted in the future. Future versions of the FOBY will be more convenient to deploy and transport. Self-shading of the instrument will be minimized via the miniaturization of sensors.

Data Availability Statement

In situ data supporting this article are available at the following zenodo link (<https://zenodo.org/record/3979918#.XzMkzZgzaUk>).

References

- Ahn, Y., Ryu, J., & Moon, J. (1999). *Development of red tide & water turbidity algorithms using ocean color satellite*, KORDI Report No. BSPE 98721-00-1224-01 (p. 287). Seoul, Korea: KORDI.
- Babin, M., Stramski, D., Ferrari, G. M., Claustre, H., Bricaud, A., Obolensky, G., & Hoepffner, N. (2003). Variations in the light absorption coefficients of phytoplankton, nonalgal particles, and dissolved organic matter in coastal waters around Europe. *Journal of Geophysical Research*, *108*(C7), 3211. <https://doi.org/10.1029/2001JC000882>
- Castagna, A., Simis, S. G. H., Dierssen, H. M., Vanhellefont, Q., Sabbe, K., & Vyverman, W. (2020). Extending Landsat 8: Retrieval of an orange contra-band for inland water quality applications. *Remote Sensing*, *12*(4), 637. <https://doi.org/10.3390/RS12040637>
- Chen, X., Chen, L., Yu, Z., Tian, L., & Zhang, W. (2009). Chromophoric dissolved organic matter optical characteristics and spatial distribution in the lakes of the middle reaches of the Yangtze River. *Journal of Lake Science*, *21*(2), 248–254. <https://doi.org/10.18307/2009.0214>
- Cui, T., Song, Q., Tang, J., & Zhang, J. (2013). Spectral variability of sea surface skylight reflectance and its effect on ocean color. *Optics Express*, *21*(21), 24,929–24,941. <https://doi.org/10.1364/OE.21.024929>
- Dunstan, P. K., Foster, S. D., King, E., Risbey, J., O'Kane, T. J., Monselesan, D., et al. (2018). Global patterns of change and variation in sea surface temperature and chlorophyll a. *Scientific Reports*, *8*(1), 14624. <https://doi.org/10.1038/s41598-018-33057-y>
- Dutkiewicz, S., Hickman, A. E., Jahn, O., Henson, S., Beaulieu, C., & Monier, E. (2019). Ocean colour signature of climate change. *Nature Communications*, *10*(1), 578. <https://doi.org/10.1038/s41467-019-08457-x>

Acknowledgments

This work was supported by the National Key R&D Program of China (Grants 2018YFB0504900, 2018YFB0504904, 2016YFC0200900, and 2016YFC1400906), the startup funding from Sun Yat-sen University (52601106 and 18831102), the National Natural Science Foundation of China (Nos. 42071325, 41701379 and 41571344), Guangdong Provincial Key-Area R&D Program (42020064), Wuhan University LuoJia Talented Young Scholar project, Dragon 4 proposal ID 32442 (entitled “New Earth Observations tools for Water resource and quality monitoring in Yangtze wetlands and lakes (EOWAQYWET)”), LIESMARS Special Research Funding, the “985 Project” of Wuhan University, and Special funds of State Key Laboratory for equipment. Special thanks are given to Prof. Zhongping Lee (University of Massachusetts, Boston) for his suggestion and encouragements of this work. We would also like to thank Guangzhou Water Color Ocean Technology Co., Ltd (www.guangzhouhoushuise.com) for their assistance in system development. Thanks Prof. Yingcheng Lu from Nanjing University, Prof. Tingwei Cui from Sun Yat-Sen University, and Prof. Jian Li from Nanjing University of Information Science & Technology for their comments on this paper.

- Garaba, S. P., & Dierssen, H. M. (2018). An airborne remote sensing case study of synthetic hydrocarbon detection using short wave infrared absorption features identified from marine-harvested macro- and microplastics. *Remote Sensing of Environment*, 205, 224–235. <https://doi.org/10.1016/j.rse.2017.11.023>
- Garaba, S. P., & Zielinski, O. (2013). Comparison of remote sensing reflectance from above-water and in-water measurements west of Greenland, Labrador Sea, Denmark Strait, and west of Iceland. *Optics Express*, 21(13), 15,938–15,950. <https://doi.org/10.1364/OE.21.015938>
- Gitelson, A. A. (1993). Nature of the peak near 700-nm on the radiance spectra and its application for remote estimation of phytoplankton pigments in inland waters. In *Proceedings of SPIE* (pp. 170–179). Tel Aviv, Israel: SPIE. <https://doi.org/10.1117/12.150992>
- Gordon, H. R., & Ding, K. (1992). Self-shading of in-water optical instruments. *Limnology and Oceanography*, 37(3), 491–500. <https://doi.org/10.4319/lo.1992.37.3.0491>
- Gregg, W. W., Casey, N. W., & McClain, C. R. (2005). Recent trends in global ocean chlorophyll. *Geophysical Research Letters*, 32, L03606. <https://doi.org/10.1029/2004gl021808>
- Groom, S., Sathyendranath, S., Ban, Y., Bernard, S., Brewin, R., Brotas, V., et al. (2019). Satellite ocean colour: Current status and future perspective. *Frontiers in Marine Science*, 6(485). <https://doi.org/10.3389/fmars.2019.00485>
- Hooker, S. B., Lazin, G., Zibordi, G., & McLean, S. (2002). An evaluation of above- and in-water methods for determining water-leaving radiances. *Journal of Atmospheric and Oceanic Technology*, 19(4), 486–515. [https://doi.org/10.1175/1520-0426\(2002\)019<0486:aeoaa1>2.0.co;2](https://doi.org/10.1175/1520-0426(2002)019<0486:aeoaa1>2.0.co;2)
- Hooker, S. B., & Maritorena, S. (2000). An evaluation of oceanographic radiometers and deployment methodologies. *Journal of Atmospheric and Oceanic Technology*, 17(6), 811–830. [https://doi.org/10.1175/1520-0426\(2000\)017<0811:aeoora>2.0.co;2](https://doi.org/10.1175/1520-0426(2000)017<0811:aeoora>2.0.co;2)
- Hooker, S. B., Zibordi, G., Berthon, J.-F., & Brown, J. W. (2004). Above-water radiometry in shallow coastal waters. *Applied Optics*, 43(21), 4254–4268. <https://doi.org/10.1364/AO.43.004254>
- IOCCG (2012). *Ocean-colour observations from a geostationary orbit*. Dartmouth, Canada: IOCCG.
- Kutser, T., Birgot, P., Charles, V., Martin, L., Tuuli, S., Kaire, T., & Gema, C. (2016). Remote sensing of black lakes and using 810 nm reflectance peak for retrieving water quality parameters of optically complex waters. *Remote Sensing*, 8(6). <https://doi.org/10.3390/RS8060497>
- Kutser, T., Vahtmae, E., Paavel, B., & Kauer, T. (2013). Removing glint effects from field radiometry data measured in optically complex coastal and inland waters. *Remote Sensing of Environment*, 133(133), 85–89. <https://doi.org/10.1016/j.rse.2013.02.011>
- Lahet, F., Ouillon, S., & Forget, P. (2000). A three-component model of ocean color and its application in the Ebro River mouth area. *Remote Sensing of Environment*, 72(2), 181–190. [https://doi.org/10.1016/S0034-4257\(99\)00101-7](https://doi.org/10.1016/S0034-4257(99)00101-7)
- Leathers, R. A., Downes, T. V., & Mobley, C. D. (2001). Self-shading correction for upwelling sea-surface radiance measurements made with buoyed instruments. *Optics Express*, 8(10), 561–570. <https://doi.org/10.1364/OE.8.000561>
- Lee, Z., Ahn, Y. H., Mobley, C., & Arnone, R. (2010). Removal of surface-reflected light for the measurement of remote-sensing reflectance from an above-surface platform. *Optics Express*, 18(25), 26,313–26,324. <https://doi.org/10.1364/OE.18.026313>
- Lee, Z., Pahlevan, N., Ahn, Y.-H., Greb, S., & O'Donnell, D. (2013). Robust approach to directly measuring water-leaving radiance in the field. *Applied Optics*, 52(8), 1693–1701. <https://doi.org/10.1364/AO.52.001693>
- Lee, Z., Wei, J., Shang, Z., Garcia, R., Dierssen, H., Ishizaka, J., & Castagna, A. (2019). On-water radiometry measurements: Skylight-blocked approach and data processing appendix to IOCCG protocol series (2019). In G. Zibordi, K. J. Voss, B. C. Johnson, J. L. Mueller (Eds.), *Protocols for satellite ocean colour data validation: In Situ Optical Radiometry, IOCCG Ocean Optics and Biogeochemistry Protocols for Satellite Ocean Colour Sensor Validation* (Vol. 3.0, pp. 1–7). Dartmouth, NS, Canada: IOCCG.
- Lee, Z., Wei, J., Voss, K., Lewis, M., Bricaud, A., & Huot, Y. (2015). Hyperspectral absorption coefficient of “pure” seawater in the range of 350–550 nm inverted from remote sensing reflectance. *Applied Optics*, 54(3), 546–558. <https://doi.org/10.1364/AO.54.000546>
- Li, T. (2001). The absolute irradiant calibration of the spectrograph. *Ocean Technology*, 20(4), 26–28.
- Lin, H., Lee, Z., Lin, G., & Yu, X. (2020). Experimental evaluation of the self-shadow and its correction for on-water measurements of water-leaving radiance. *Applied Optics*, 59(17), 5325–5334. <https://doi.org/10.1364/AO.391633>
- Ma, R., Duan, H., Liu, Q., & Loisel, S. A. (2011). Approximate bottom contribution to remote sensing reflectance in Taihu Lake, China. *Journal of Great Lakes Research*, 37(1), 18–25. <https://doi.org/10.1016/j.jglr.2010.12.002>
- Marrari, M., Piola, A. R., & Valla, D. (2017). Variability and 20-year trends in satellite-derived surface chlorophyll concentrations in large marine ecosystems around south and western central America. *Frontiers in Marine Science*, 4(372). <https://doi.org/10.3389/fmars.2017.00372>
- Mason, J. D., Cone, M. T., & Fry, E. S. (2016). Ultraviolet (250–550 nm) absorption spectrum of pure water. *Applied Optics*, 55(25), 7163–7172. <https://doi.org/10.1364/AO.55.007163>
- Mobley, C. D. (1999). Estimation of the remote-sensing reflectance from above-surface measurements. *Applied Optics*, 38(36), 7442–7455. <https://doi.org/10.1364/AO.38.007442>
- Mueller, J. L. (2003). *Radiometric measurements and data analysis protocols rep*. Greenbelt, MD: Goddard Space Flight Center.
- Ritchie, R. J. (2006). Consistent sets of spectrophotometric chlorophyll equations for acetone, methanol and ethanol solvents. *Photosynthesis Research*, 89(1), 27–41. <https://doi.org/10.1007/s11120-006-9065-9>
- Ruddick, K. G., Voss, K., Boss, E., Castagna, A., Frouin, R., Gilerson, A., et al. (2019). A review of protocols for fiducial reference measurements of water-leaving radiance for validation of satellite remote-sensing data over water. *Remote Sensing*, 11(19), 2198. <https://doi.org/10.3390/rs11192198>
- Schalles, J. (2006). Optical remote sensing techniques to estimate phytoplankton chlorophyll concentrations in coastal waters with varying suspended matter and cdom concentrations. In *Remote Sensing and Digital Image Processing* (pp. 27–79). Cham: Springer International Publishing. https://doi.org/10.1007/1-4020-3968-9_3
- Shang, Z., Lee, Z., Dong, Q., & Wei, J. (2017). Self-shading associated with a skylight-blocked approach system for the measurement of water-leaving radiance and its correction. *Applied Optics*, 56(25), 7033–7040. <https://doi.org/10.1364/AO.56.007033>
- Smith, R. C., Booth, C. R., & Star, J. L. (1984). Oceanographic biooptical profiling system. *Applied Optics*, 23(16), 2791–2797. <https://doi.org/10.1364/AO.23.002791>
- Soja-Woźniak, M., Craig, S., Kratzer, S., Wojtasiewicz, B., Darecki, M., & Jones, C. (2017). A novel statistical approach for ocean colour estimation of inherent optical properties and cyanobacteria abundance in optically complex waters. *Remote Sensing*, 9(4), 343. <https://doi.org/10.3390/rs9040343>
- Tanaka, A., Sasaki, H., & Ishizaka, J. (2006). Alternative measuring method for water-leaving radiance using a radiance sensor with a domed cover. *Optics Express*, 14(8), 3099–3105. <https://doi.org/10.1364/OE.14.003099>

- Toole, D. A., Siegel, D. A., Menzies, D. W., Neumann, M. J., & Smith, R. C. (2000). Remote-sensing reflectance determinations in the coastal ocean environment: Impact of instrumental characteristics and environmental variability. *Applied Optics*, *39*(3), 456–469. <https://doi.org/10.1364/AO.39.000456>
- Visser, F., Buis, K., Verschoren, V., & Meire, P. (2015). Depth estimation of submerged aquatic vegetation in clear water streams using low-altitude optical remote sensing. *Sensors*, *15*(10), 25,287–25,312. <https://doi.org/10.3390/s151025287>
- Wei, J., Lee, Z., Garcia, R., Zoffoli, L., Armstrong, R. A., Shang, Z., et al. (2018). An assessment of Landsat-8 atmospheric correction schemes and remote sensing reflectance products in coral reefs and coastal turbid waters. *Remote Sensing of Environment*, *215*, 18–32. <https://doi.org/10.1016/j.rse.2018.05.033>
- Wei, J., Lee, Z., Lewis, M. R., Pahlevan, N., Ondrusek, M., & Armstrong, R. A. (2015). Radiance transmittance measured at the ocean surface. *Optics Express*, *23*(9), 11,826–11,837. <https://doi.org/10.1364/OE.23.011826>
- Wei, J., Lee, Z., & Shang, S. (2016). A system to measure the data quality of spectral remote-sensing reflectance of aquatic environments. *Journal of Geophysical Research: Oceans*, *121*, 8189–8207. <https://doi.org/10.1002/2016JC012126>
- Yadav, S., Yoneda, M., Susaki, J., Tamura, M., Ishikawa, K., & Yamashiki, Y. (2017). A satellite-based assessment of the distribution and biomass of submerged aquatic vegetation in the optically shallow basin of Lake Biwa. *Remote Sensing*, *9*(9), 966. <https://doi.org/10.3390/rs9090966>
- Zhang, X. (1998). On the estimation of biomass of submerged vegetation using Landsat thematic mapper (TM) imagery: A case study of the Honghu Lake, PR China. *International Journal of Remote Sensing*, *19*(1), 11–20. <https://doi.org/10.1080/014311698216396>
- Zhao, J. (2010). *A study on the natural fluorescence of phytoplankton, doctorate degree thesis*. Guangzhou, China: South China Sea Institute of Oceanology, Chinese Academy of Sciences.
- Zhao, J., Cao, W., Xu, Z., Ai, B., Yang, Y., Jin, G., et al. (2018). Estimating CDOM concentration in highly turbid estuarine coastal waters. *Journal of Geophysical Research: Oceans*, *123*, 5856–5873. <https://doi.org/10.1029/2018JC013756>
- Zhou, Z., Tian, W., & Mei, X. (2017). Quantitative retrieval of chlorophyll-a concentration by remote sensing in Honghu Lake based on Landsat8 data. *Journal of Hubei University (Natural Science)*, *39*(2), 212–216.
- Zibordi, G., Hooker, S. B., Berthon, J. F., & D'Alimonte, D. (2002). Autonomous above-water radiance measurements from an offshore platform: A field assessment experiment. *Journal of Atmospheric and Oceanic Technology*, *19*(5), 808–819. [https://doi.org/10.1175/1520-0426\(2002\)019<0808:AAWRMF>2.0.CO;2](https://doi.org/10.1175/1520-0426(2002)019<0808:AAWRMF>2.0.CO;2)
- Zibordi, G., Mélin, F., Berthon, J. F., Holben, B., Slutsker, I., Giles, D., et al. (2009). AERONET-OC: A network for the validation of ocean color primary products. *Journal of Atmospheric and Oceanic Technology*, *26*(8), 1634–1651. <https://doi.org/10.1175/2009jtecho654.1>
- Zibordi, G., Melin, F., Hooker, S. B., Alimonte, D. D., & Holben, B. (2004). An autonomous above-water system for the validation of ocean color radiance data. *IEEE Transactions on Geoscience and Remote Sensing*, *42*(2), 401–415. <https://doi.org/10.1109/TGRS.2003.821064>
- Zibordi, G., Mélin, F., Voss, K. J., Johnson, B. C., Franz, B. A., Kwiatkowska, E., et al. (2015). System vicarious calibration for ocean color climate change applications: Requirements for in situ data. *Remote Sensing of Environment*, *159*, 361–369. <https://doi.org/10.1016/j.rse.2014.12.015>
- Zibordi, G., & Talone, M. (2020). On the equivalence of near-surface methods to determine the water-leaving radiance. *Optics Express*, *28*(3), 3200–3214. <https://doi.org/10.1364/OE.28.003200>